Assessment Measures for Hybrid Simulation: A Discussion of Recent Developments

R. Mirza Hessabi
Department of Civil Engineering, University of Toronto

O. Mercan
Department of Civil Engineering, University of Toronto

ABSTRACT: Recently, a summary of some of the available assessment measures that can be implemented by users to evaluate the accuracy of a hybrid simulation was published in the NEEShub [1]. The current document reviews two more sets of tracking measures, namely, Phase and Amplitude Error Indices (PAEI) and frequency domain-based (FDB) error indicators that can be successfully used as a post-processing tool. PAEI and FDB do not use test setup specific parameters and as such, can be used as standard tools for assessing the quality of the experiments performed in different laboratories or under different conditions. Additionally, FDB error indicators use uncomplicated mathematical functions, which make them suitable for implementation in real-time hybrid simulation. They been already implemented and experimentally verified as online indicators and have been incorporated into an adaptive servo-hydraulic control loop. In this document, through several numerical and experimental simulations, the capabilities of PAEI and FDB indicators in assessing the success of hybrid simulations are demonstrated.

1. INTRODUCTION

Several potential experimental and numerical error sources such as the truncation errors, communication delays and inherent actuator dynamics can result in undesirable differences between the command and measured signals in hybrid simulation [1]. This is of major importance because it has been previously shown that hybrid simulation is vulnerable to error propagation, which can affect the accuracy and even the stability of the entire experiment [2]. Since it is not always possible to have shake table or accurate theoretical results for comparison and assessment of the quality of the hybrid simulations, it is imperative to employ efficient measures to establish the reliability of the experiments.

In [1], the available assessment measures from the literature are mainly categorized into two classes of local and global response assessment measures. As such, the main focus of the local response assessment methods is to evaluate the accuracy of the synchronization of the numerical and physical components and various time domain, frequency domain and energy-based analyses [1] are performed to measure the actuator tracking error (i.e. inability of the hydraulic actuators to attain the command displacements during the specified time interval). Fig. 1 illustrates the difference between command and measured displacements in hybrid simulation. Mercan and Ricles [3], independent of a particular integration algorithm, investigated the accuracy and stability characteristics of the outer loop dynamics of real-time pseudodynamic tests. They concluded that in comparison to other types of errors, the delay (i.e. phase lag) in the measured signals is more critical as it introduces additional energy into the system and causes instability in the outer loop dynamics. Consequently, it is crucial to develop error indicators that are capable

of decoupling various types of tracking errors (i.e. phase and amplitude errors) and can be implemented and executed in real-time. The latter enables the error indicators to be used online to monitor the actuator tracking as the simulation progresses.

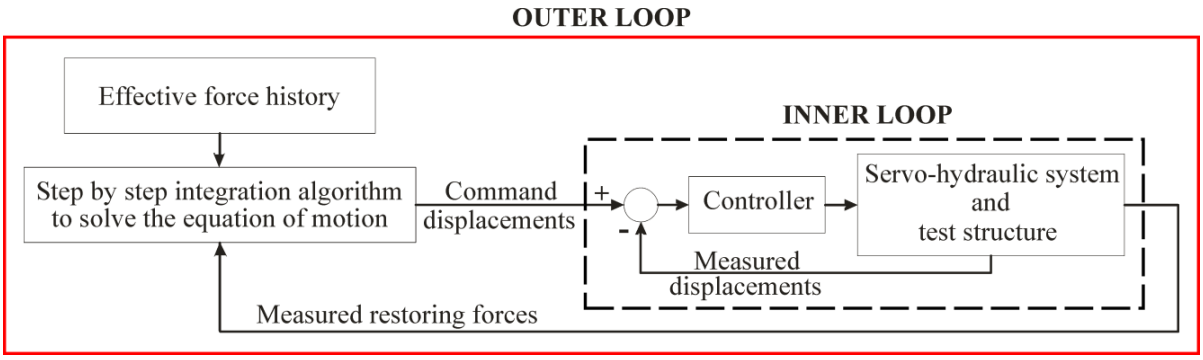

Fig. 1. Block diagram for a hybrid simulation [3].

In the following sections, the equations for the PAEI and FDB error indicators are introduced and then through numerical and experimental studies, the accuracies of these error indicators in quantifying the tracking errors are investigated. In addition, their performances are compared to other local response assessment measures listed in [1].

2. FORMULATION OF PAEI AND FDB ASSESSMENT MEASURES

2.1. PHASE AND AMPLITUDE ERROR INDICES (PAEI)

In 2012, to account for the problems with previous assessment measures, based on the characteristics of the Synchronization Subspace Plots (SSPs) of command and measured displacements, Mirza Hessabi and Mercan proposed PAEI [3]. SSPs have the measured signal (i.e., displacements) plotted against the commands, and are used in signal processing. In Fig.2 (a), for one cycle of command displacement (referred to as command), the measured displacements are considered to have overshoot and undershoot amplitude error (indicated as overshoot and undershoot, respectively). In Fig. 2(b), it can be seen that for the perfect tracking case (i.e., when the measured displacements are exactly the same as the commands), the SSP is a straight line with 45° inclination. With overshoot amplitude error, the inclination angle of the SSP is greater than 45°, and similarly with the undershoot error it is less than 45°. Fig. 2(c) considers phase errors in the form of lead and lag as indicated. When there is a phase error in the measured displacement, the SSP is no longer a straight line, but it exhibits elliptical hysteresis. The hysteresis loops evolve clockwise in the presence of phase lead and they evolve counterclockwise when there is a phase lag in the measured displacement (see Fig. 2(d)). Fig. 3 shows the command and measured displacements from a real-time PSD test (Fig. 3(a)), and the corresponding SSP (Fig. 3(c)). As can be seen in the enlarged view in Fig. 3(b) there are amplitude and phase errors in the measured displacements superimposed with the noise. The effect of the noise in the SSP can be observed better in the enlarged view in Fig. 3(d).

SSPs were also employed by Mercan and Ricles [4] and the enclosed area by these plots was used in the formulation of Tracking Indicators (TIs). However, instead of computing the

enclosed areas, in the derivation of PAEI, a least square fitting method was used to fit the data points of the SSP at a given time window to the equation of an ellipse described by Equation 1.

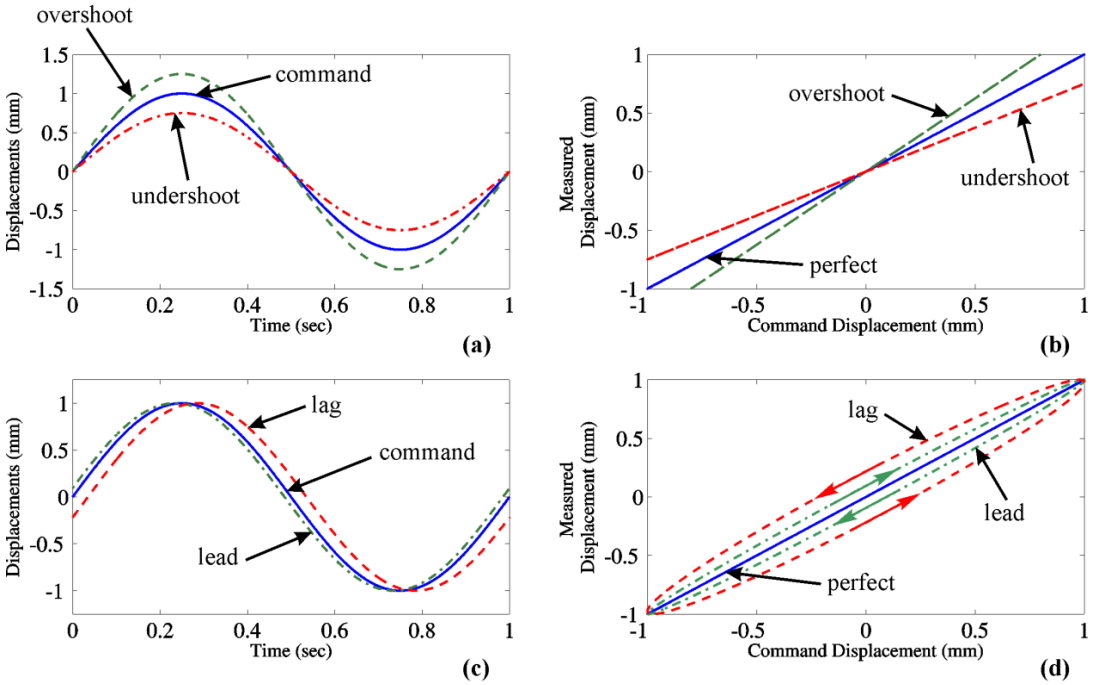

Fig. 2. Sinusoidal actuator displacement time histories and associated SSPs [3].

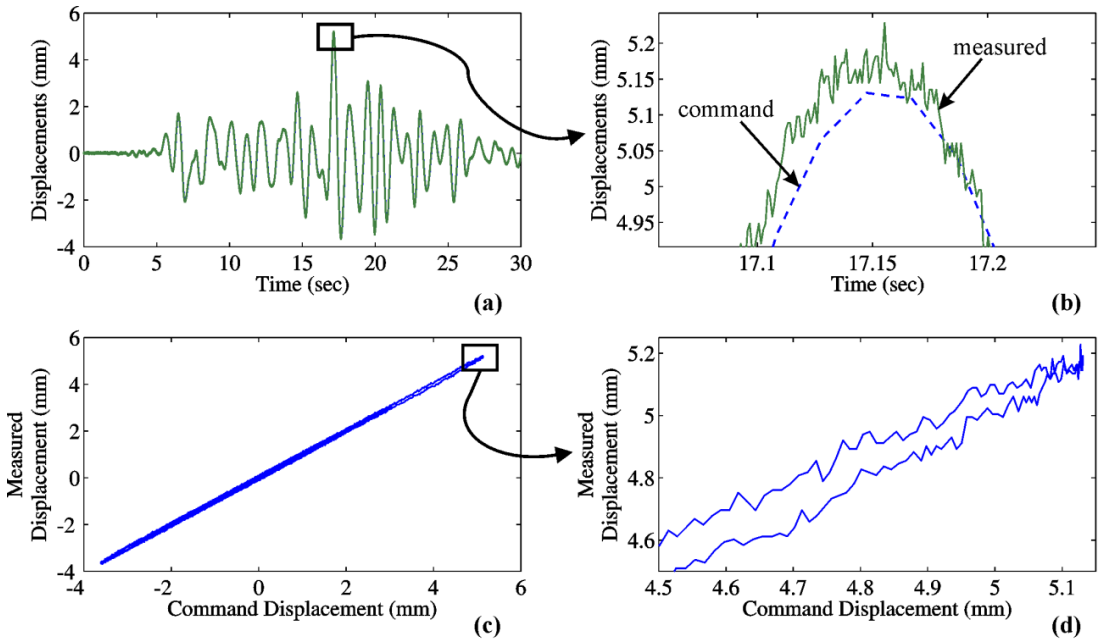

Fig. 3. Displacement time histories of real experiment and associated SSPs [3].

These equations of the ellipses as they evolve and appear in the synchronization subspace are directly correlated to the phase and amplitude errors in the corresponding time windows.

$$aD_c^2 + bD_cD_m + cD_m^2 + dD_c + eD_m + f = 0 \quad (1)$$

where, D_c and D_m are command and measured displacements, respectively and a, b, c, d, e and f are the ellipse parameters that should be determined from the fitting process.

The correlation between the parameters of the fitted ellipse and phase and amplitude errors (ϕ and ΔA, respectively), are shown in Equations 2 and 3:

$$\phi = \left| arccos\left(\frac{b}{2\sqrt{c}}\right)\right| \tag{2}$$

$$\Delta A = \sqrt{\left|\left(\frac{f}{sin^2(\phi)}\right)\right|}\left\{1 - \frac{1}{\sqrt{c}}\right\} \tag{3}$$

In the above equations, an amplitude ratio (ΔA) is defined as the ratio of the command over measured displacement amplitudes. Similarly, a phase error (ϕ) is defined based on the discrepancy of the phase shifts between the command and measured signals. For the amplitude error, the obtained value of ΔA in Equation 3 readily determines the type of the error, where, a value greater than one is an indication of undershoot error and a value less than one represents overshoot. On the other hand, the phase error determined by Equation 2 is always a positive quantity. To distinguish a negative phase error (i.e., lag) from a positive one (i.e., lead) the proper sign needs to be introduced. This is done by using the angle accumulated within each time window. The angle accumulated is computed in such a way that it is a positive quantity when the SSP evolves clockwise (e.g., phase lead behaviour) and is negative for the opposite evolution of the SSP (e.g., phase lag behaviour) for the time window considered. Thus, the sign of the accumulated angle readily determines the correct sign for the phase error. It should be added that in the formulation of PAEI, a moving time window approach is adopted, where for the *i*th step at time t_i (i.e., $((D_c)_i, (D_m)_i)$), in addition to this last point on the SSP, an appropriate number of previous data points are considered. To determine the proper size of the time window, recommendations provided in [3] can be used.

Fig. 4 introduces the flowchart that explains the implementation of the required steps for calculating PAEI. The definition of the parameters appeared in the flowchart can be found in [3]. As can be seen in the flowchart, the very first time window needs special consideration. The process starts with a predefined number of initial data points followed by ellipse fitting. In each iteration step, the center of the fitted ellipse is computed and checks to determine the proper size of the time window are performed. For the very first window, when these checks are not satisfied, one more data point is added marching forward in time (i.e., the end index of the data subset array is modified). The steps are the same for all the consequent time windows, the only difference is that each new data point is added going backwards in time (i.e., the start index of the data subarray is modified). This way, PAEI has the potential to be applied online for processing the data in real-time as the test progresses. Once each time window converges, the phase and amplitude errors are computed using the closed-form relationships presented in Equations 2 and 3, and they are recorded.

2.2. FREQUENCY DOMAIN-BASED ERROR INDICATORS (FDB)

Despite of being accurate, the calculation of PAEI involves solving large eigenvalue problems at each time step and therefore it is relatively computationally expensive. This limitation does not threaten the performance of PAEI as post-processing assessment tools but it makes it difficult to use them in real-time hybrid simulation as online indicators. To overcome this limitation, Mirza Hessabi et al. [5] proposed a new set of measures that were still able to uncouple the phase

and amplitude errors and quantify them but unlike PAEI, these could be implemented and executed in real-time and served as online indicators.

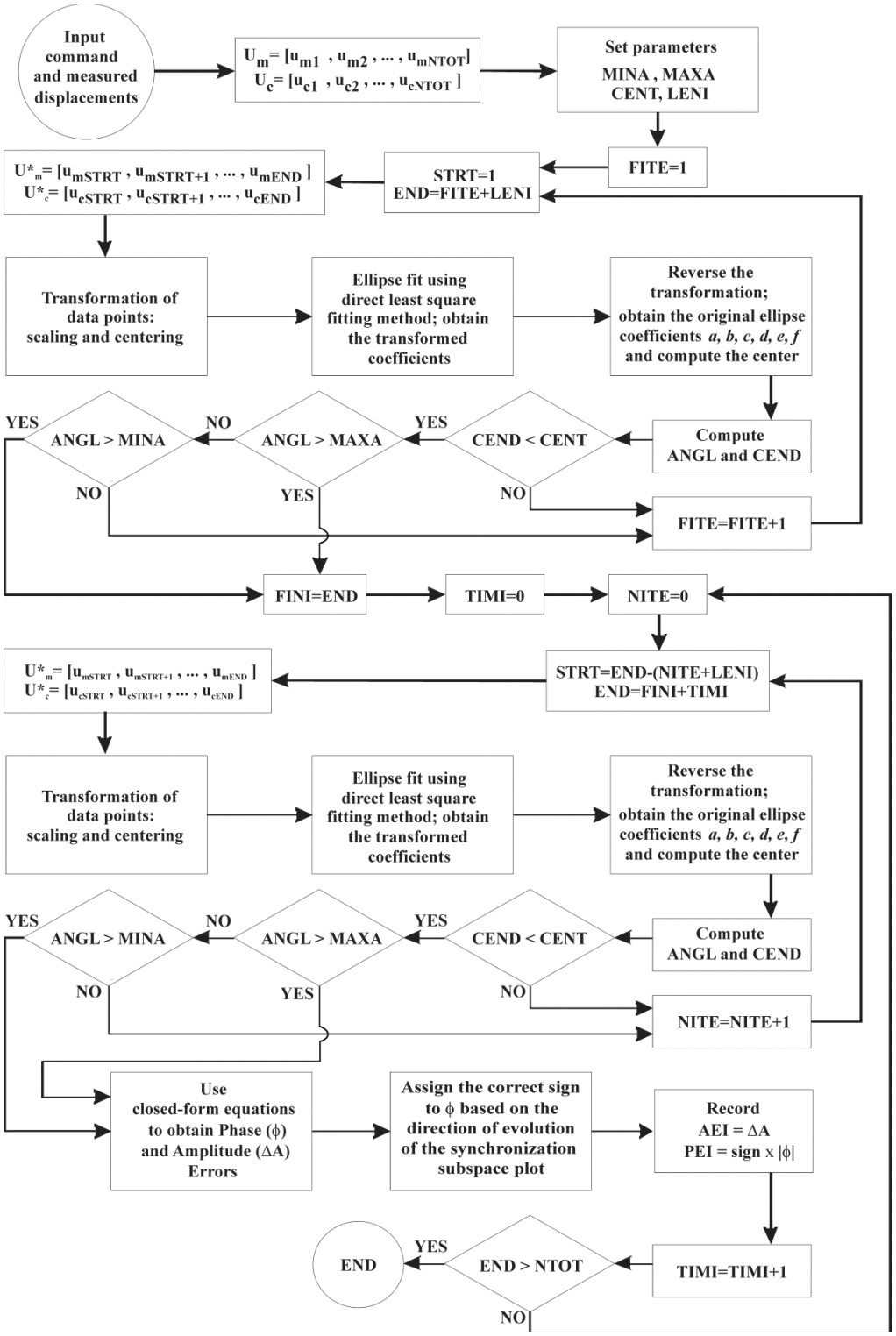

Fig. 4. Flowchart for the implementation of PAEI [3].

For the calculation of the FDB error indicators, the same time windowing approach as described in the previous section was used. In addition to some differences in their formulations, this windowing procedure distinguishes FDB indicators from the Frequency Evaluation Index (FEI) developed by Guo et al. [6]. FDB error indicators are derived using discrete Fourier transforms (DFTs). By definition, the DFT spectrum is a periodical spectrum and is discrete in frequency domain. To obtain the FDB error indicators, first the DFT power spectra need to be calculated for the command and measured signals independently. Then, from each power spectrum, the frequency that corresponds to the largest amplitude is located (i.e. $\bar{f}_c$ and $\bar{f}_m$ for command and measured signals, respectively). As shown in Equation 4, the ratio between the magnitudes of the power spectra at the frequencies of $\bar{f}_c$ and $\bar{f}_m$ can be used to determine the amplitude ratio,

$$\Delta A = \left|U_c(\bar{f}_c)\right| / \left|U_m(\bar{f}_m)\right| \tag{4}$$

Likewise, the phase error is found as the difference of the DFT phase spectrum values of the two signals at $\bar{f}_c$ and $\bar{f}_m$.

$$\phi = \phi_c^*(\bar{f}_c) - \phi_m^*(\bar{f}_m) \tag{5}$$

Similar to PAEI, positive and negative phase error values from Equation 5 show phase lead and lag, respectively. Moreover, a value greater than one obtained from Equation 4 is an undershoot error and a value less than one represents overshoot. Moreover, it should be emphasized that the closer ΔA and ϕ values are to 1 and 0, respectively, the more accurate is the actuator control and the more reliable are the simulation results. In order to implement FDB error indicators as online indicators that assess the error as a function of time as the real-time hybrid simulation progresses, the DFT spectra are obtained and a windowing approach is employed. To reduce spectral leakage effects, windowing functions (e.g. Han, Hamming windows) should be used and special care should be taken about the DC component of the frequency response.

3. COMPARISON WITH OTHER LOCAL RESPONSE ASSESSMENT MEASURES

As it is listed in [1], there are several other local response assessment measures. In this section, differences between these measures and the two types of indicators that are reviewed in this paper (i.e., PAEI and FDB error indicators) are explained. Using numerical and experimental case studies, quantitative comparisons between these measures are shown in Section 4.

A normalized root mean square in experiment (NRMSE) is the first time domain based measure that will be discussed in this section [7, 8]. Although NRMSE provides valuable qualitative insights into actuator tracking (in terms of the difference between the measured and command displacements), it often fails to provide quantitative assessment into the effects of actuator delay due to their dependence on the response history [6]. On the other hand, the cross correlation between the target and measured displacement can be used to estimate the actuator delay. However, the cross correlation between the target and measured displacement fails to provide quantitative assessment into the effects of the amplitude error.

Energy methods such as Hybrid Simulation Error Monitors (HSEM) [9, 10] and energy error indicator (EEI) [11] were introduced to use energy parameters to quantify the difference between

actual experimental behavior and that observed in explicit numerical simulations. These indicators estimate errors associated with phase (i.e., lead/lag) but they do not address the amplitude errors. As such, in the presence of both amplitude and phase errors, the energy-based indicator lumps these two types of errors together. Moreover, energy methods are influenced by the structural model and ground motion considered. For instance, to assess the accuracy of a given test result and establish an acceptable threshold for HSEM, numerical simulations that determine a relationship between the accuracy measures and HSEM need to be carried out and as a result, energy methods can be considered as test structure/experiment specific. This implies that the values of energy-based indicators obtained from two different tests with considerably different command displacement histories and/or different test structures cannot directly be compared to each other. On the other hand, PAEI and FDB error indicators do not use test setup specific parameters in their formulation, and can quantify the errors independent of the amplitude of the command displacements. As such, PAEI and FDB error indicators can be used as a standard tool for assessing the quality of the experiments performed in different laboratories or under different conditions.

Another tool for assessing the actuator tracking performance in hybrid simulations is the Tracking Indicator (TI) [4] in which the areas enclosed by the SSPs are used. Similar to energy methods, although TI is useful in evaluating the test results, it cannot determine the amplitude and phase errors separately and is affected by the amplitude of the command displacements. As such, it cannot serve as a standard assessment tool for the real-time test results.

Through numerical and experimental simulations, the abovementioned differences are shown in the next Section.

4. NUMERICAL AND EXPERIMENTAL CASE STUDIES

4.1. PHASE AND AMPLITUDE ERROR INDICES (PAEI)

To evaluate the performance of PAEI, four different cases summarized in Table 1 are considered. As will be discussed in detail later, comparisons of tracking evaluation with HSEM, TI and PAEI are provided using numerical simulations, and also real experimental data (Case (iv)).

4.1.1. Case (i)

In Case (i) predefined displacement command (Equation 6) and measured (Equation 7) signals with known phase and amplitude errors are processed using PAEI.

$$\mathrm{u_c} = \mathrm{A_c} \times \cos(3\pi t) \tag{6}$$

$$\mathrm{u_m} = \mathrm{A_m} \times \cos(3\pi\,[t + 15 \times \Delta t]) \tag{7}$$

where, t is time, Δt is the size of time steps and is equal to 1/1024 seconds (which is the clock speed of a typical digital controller), u_c and u_m represents command and measured displacements, respectively. Also, A_c and A_m refer to the amplitudes of the command and measured displacements. In this case, A_c and A_m are assumed 1.5 and 2.0 mm, respectively. As can be seen from Equations 6 and 7 (and also summarized in Table 1), there is a constant overshoot error of 0.5 mm in the measured displacement, and a time lead of 15 time steps. Note that, considering

the frequency of the signals (i.e., $\omega = 3\pi$) this time lead corresponds to a phase lead of 0.1381 rad (i.e. $\emptyset = \frac{3\pi \times 15}{1024} = 0.1381\, rad$).

Table 1.Cases considered in the performance evaluation of the tracking indicators [3]

	Description	Input Force (kN)	Introduced time shift	Introduced amplitude error	Nonlinearity	Noise
Case(i)	Predefined displacement signals	-----	15 time steps (lead)	- 0.5 mm (overshoot)	No	No
Case (ii-a)	Simulink model	$50 \times \sin(2\sqrt{2}\pi \times \frac{t}{T_n})$	5 time steps (lag)	10% overshoot ($-0.1 \times A_c$)	No	No
Case (ii-b)		$100 \times \sin(2\sqrt{2}\pi \times \frac{t}{T_n})$				
Case(iii)	Simulink model	$100 \times \sin(2\sqrt{2}\pi \times \frac{t}{T_n})$	-5 time steps (lag)	$0 < t < 5$s: 10% overshoot ($-0.1 \times A_c$) $5 < t < 10$s: 25% undershoot ($0.25 \times A_c$)	Yes	Yes
Case (iv)	Experimental data	Canoga Park earthquake ground acceleration	-----	-----	Yes	Yes

Fig. 5(a) shows the command and measured displacements for Case (i) for 6 seconds, where the corresponding SSP is provided in Fig. 5(b). A closer look at the PAEI in Fig. 5(c) and (d) shows that the phase and amplitude errors are identified exactly. It should be noted that Case (i) represents a highly ideal case, where the signals involved has a constant frequency, constant phase and amplitude errors and in the absence of any nonlinear or noise effects.

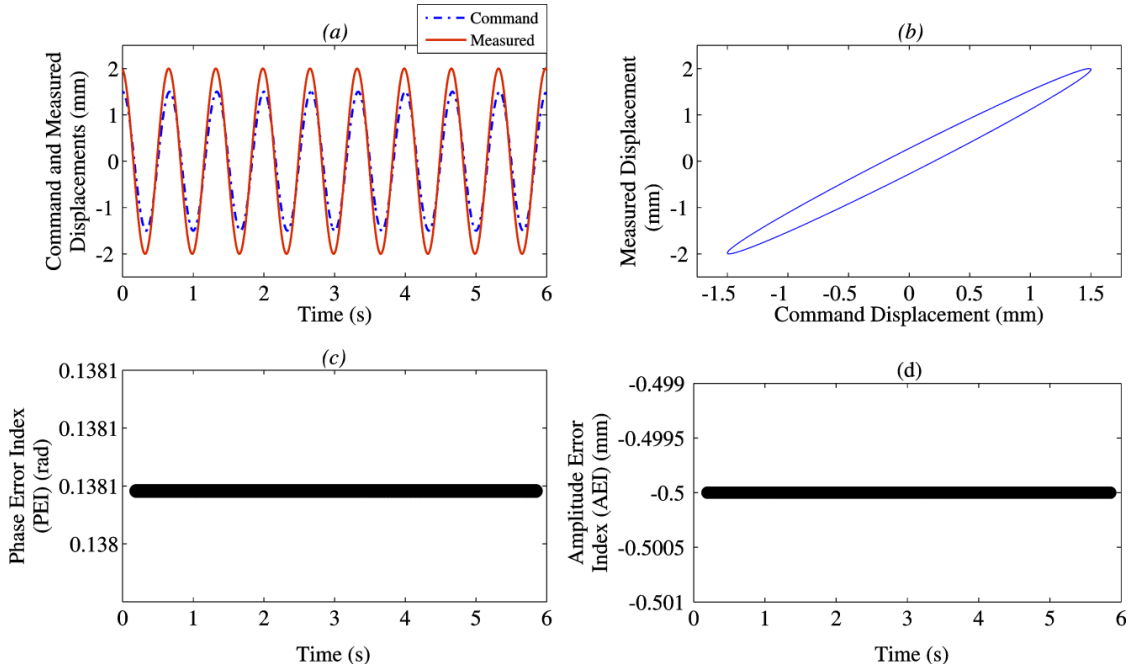

Fig. 5. Tracking Evaluation with PAEI for Case (i) [3]

4.1.2. Case (ii)

In Case (ii), the command displacements (indicated as *uc* in Fig. 6) are generated by solving the equation of motion of a single-degree-of-freedom (SDOF) structure using the MATLAB Simulink model shown in Fig. 6.

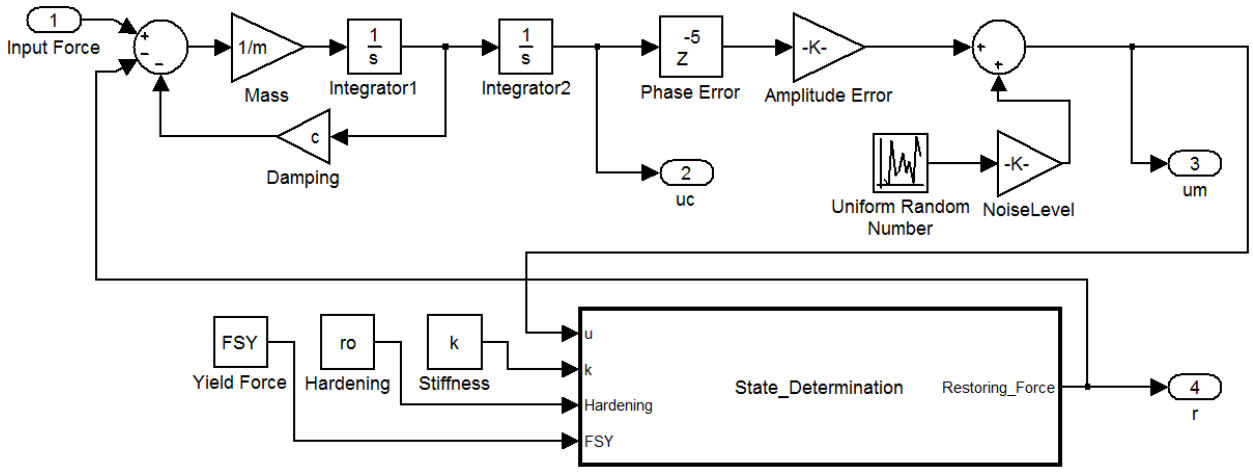

Fig. 6. Simulink model used in Cases (ii) and (iii) [3]

The measured displacements (indicated as *um* in Fig. 6) are then obtained by introducing an integer delay block from the Simulink library for the phase error, a multiplier (gain) block to introduce the amplitude error and a random number generator to consider the noise effects. As can be seen from Table 1, the integer delay block z^{-5} provides a time lag of 5 time steps, where the time step size is set by the Simulink solver (in this case 0.001 sec.). Setting the gain value as 1.1, a 10% overshoot amplitude error is introduced in the measured displacement. The restoring force characteristics of the SDOF are captured in the embedded function with the name "State determination" where an elastic-perfectly plastic spring with strain hardening is programmed. By adjusting the value of the yield parameter this spring can be made to respond linearly as well. The numerical values of the parameters that are used in representing the SDOF system are given in Table 2.

Table 2. Properties of the SDOF structure [3]

Stiffness (k) (kN/m)	Undamped Natural Period (T_n) (sec)	Damping Coefficient ζ	Yield Displacement Δy (mm)		Strain Hardening (ρ)	
			Linear	Nonlinear	Linear	Nonlinear
11500	1.15	0.02	---	10	---	0.01

As noted previously, HSEM requires the measured restoring force to evaluate tracking performance. In Case (ii) by using the Simulink model to solve the equation of motion with the state determination process, the restoring force becomes readily available which in turn makes it possible to have a comparison between HSEM, TI and PAEI. In Case (ii), the structure is assumed to be linear, there is no noise, and the above mentioned phase and amplitude errors are

present in the measured displacements. The only difference between Case (ii-a) and Case (ii-b) is the amplitude of the forcing function. Since the amplitude of the applied force is twice as much in Case (ii-b) as in Case (ii-a), the resulting displacements in Case (ii-b) have twice larger amplitudes compared to Case (ii-a) (See Fig. 7 (a) and (b)). This is expected as a linear dynamic system is simulated under two different level of force with everything else being the same. Fig.7(c) and (d) show the resulting SSP's where the latter has the same major axis inclination but is bigger as a result of the larger displacements involved. The restoring force-displacement plots provided in Fig. 7(e) confirms that the structure behaves linear elastically.

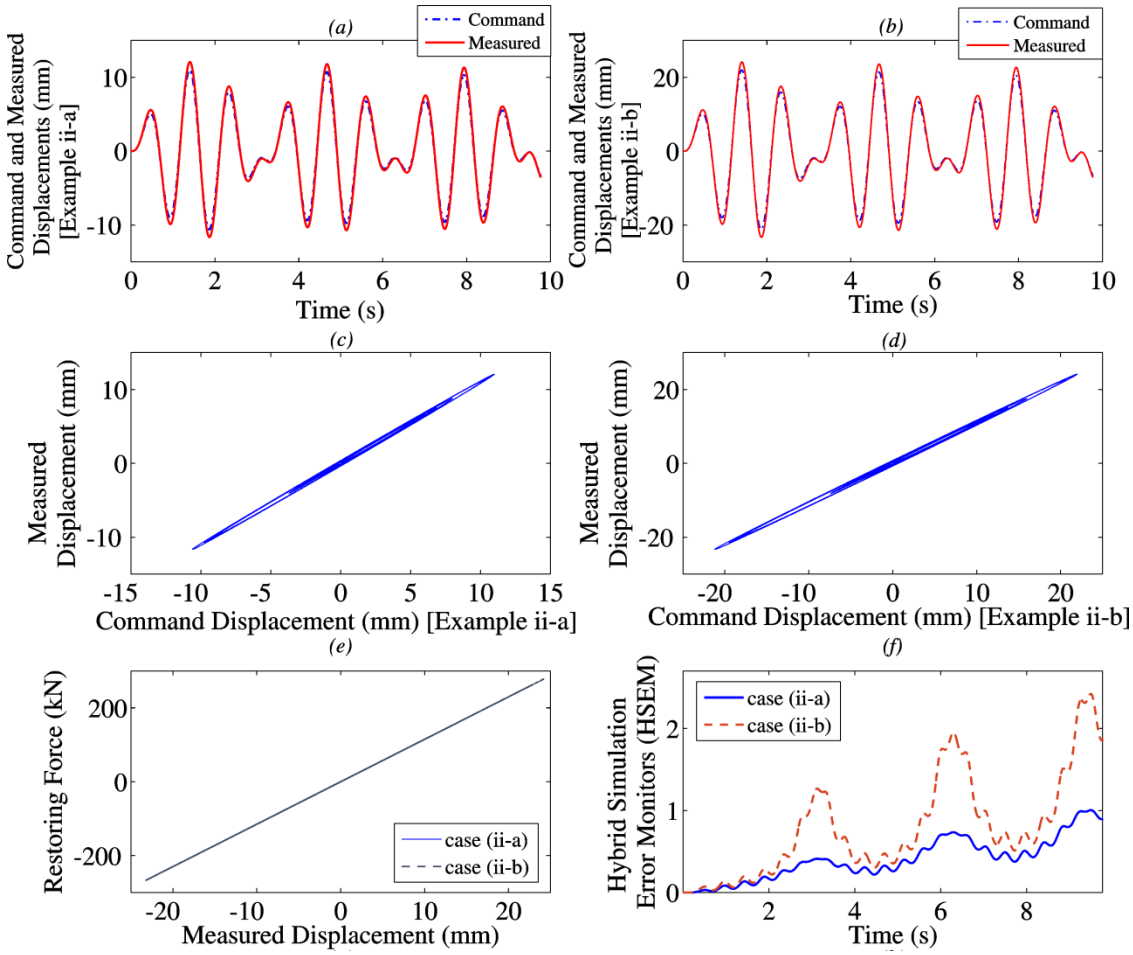

Fig. 7. Tracking evaluation comparisons with PAEI, HSEM and TI for Case (ii) [3]

Although the exact same errors are present in both cases, the tracking evaluations performed by using HSEM and TI (Fig. 7(f) and 7(g)) erroneously indicate larger errors for Case (ii-b). This is attributed to the formulation of both of these methods. HSEM is based on the energy error between the hysteresis loops of measured restoring force and measured and desired displacements respectively (i.e., E^{error}). When the command displacement amplitudes increase, even if the error between the command and measured signals remains the same, the energy error increases (simply because the hysteresis loops involved get larger). Although the normalization terms (i.e., strain energy and input energy) are introduced in the denominator of HSEM, as Case (ii) reveals, HSEM results are still affected by the amplitude of the command displacements.

Similarly, TI results are affected when the size of the SSPs change as a result of the change in the amplitude of the displacements involved (even though the errors between them remain unchanged).

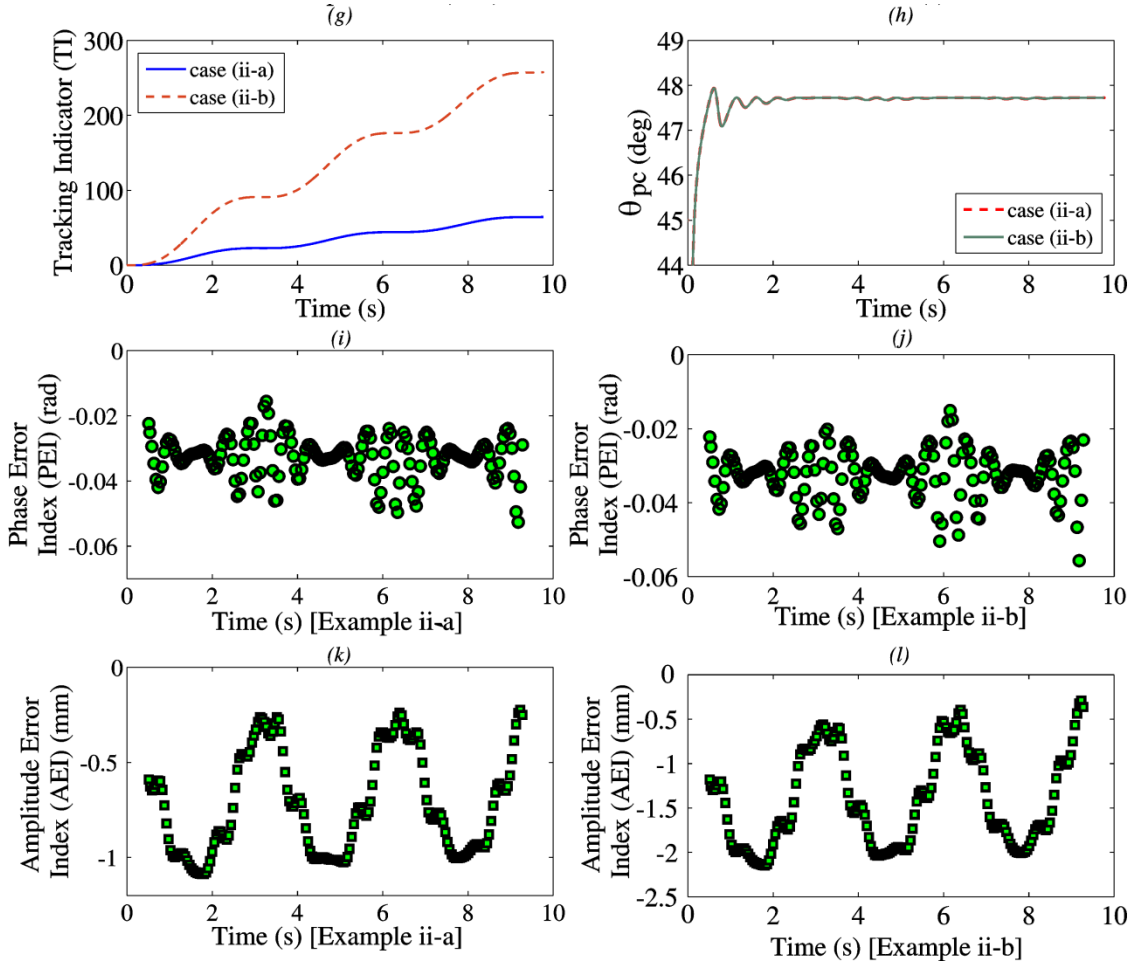

Fig.7 (Continued). Tracking evaluation comparisons with PAEI, HSEM and TI for Case (ii) [3]

Figures 7(i) through (l) show that PAEI do not suffer from the same limitation. Again, this is attributed to the formulation of the proposed indices: rather than the enclosed areas (either under the hysteresis loops or SSPs), PAEI directly uses the closed-form relationships between the ellipse coefficients and the phase and amplitude errors. In Case (ii) the command displacements are obtained by solving the equation of motion of an underdamped SDOF system subject to a sinusoidal forcing function. As a result, the transient and steady state components of the resulting displacements will contain the forcing frequency and natural frequency of the structure. Considering these frequencies, the delay introduced in time domain (i.e., 5 time steps) translates into 0.03 rad, and 0.02 rad of phase lags, respectively. As can be seen in Fig. 7(i) and (j), in both Case (ii-a) and Case (ii-b) the PEI is able to exhibit phase values around this range. Also, as the amplitude error in the measured displacements are introduced as a percentage (10%) of the command displacement in both cases, the overshoot errors are expected to roughly range from 0 to 1 mm. in Case (ii-a) and from 0 to 2mm. in Case (ii-a). In Fig. 7(k) and (l) the amplitude errors identified are in the expected range.

4.1.3. Case (iii)

Case (iii) studies the tracking evaluation in the presence of nonlinearity in the structural response, noise and a sudden change in error in the measured signal (in this case a change from overshoot to undershoot amplitude error). Simulink model presented in Fig. 6 is used where the errors provided in Table 1 are present in the measured signal.

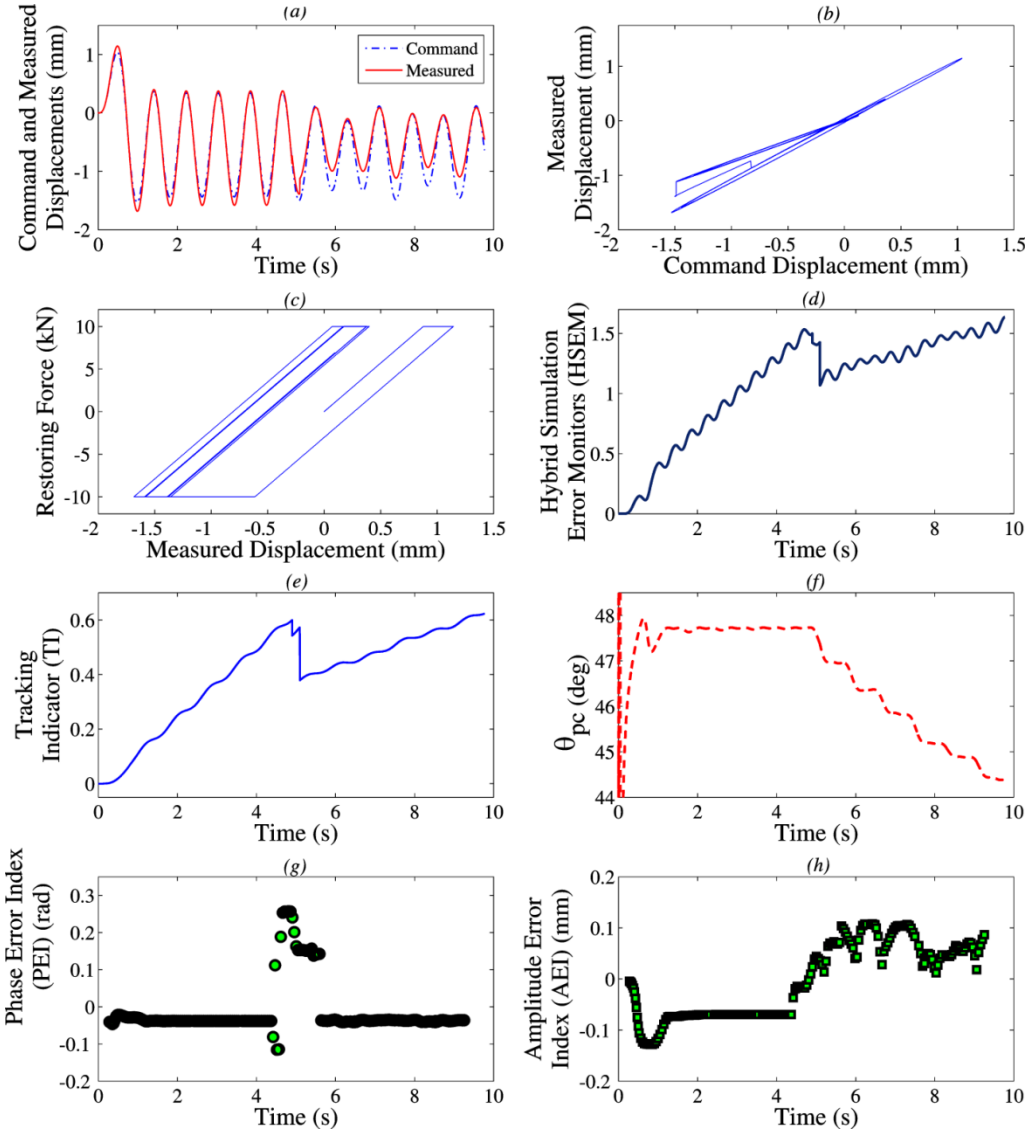

Fig. 8. Tracking evaluation comparisons with PAEI, HSEM and TI for Case (iii) [3]

As typical for the nonlinear dynamic response of the structures, the command displacement history provided in Fig. 8(a) oscillates about a non-zero position after the yielding phenomenon takes place (see Fig. 8(c)). Also, there is a sudden change in the amplitude error introduced; it switches from overshoot to undershoot suddenly at 5 seconds. Although not very realistic (even if such a switch were to occur in a real experiment, it would do so gradually over a period of time), the change in the error, together with the displacement history that oscillates about a

nonzero position result in SSPs that move around and rotate in the synchronization subspace (see Fig. 8(b)), As such, Case (iii) is a challenging scenario for PAEI where the centering and scaling transformations introduced in the formulation will be put to test.

In Fig. 8 (d) and (e) both HSEM and TI are able to qualitatively indicate the presence of the existence of the time delay, where, as a result of the use of the transpose areas in its formulation, TI is less sensitive to the presence of the noise. Fig. 8 (g) and (h) show that PAEI successfully quantify the phase and amplitude errors. Note that in the results from all the indicators, there is a distortion around the time where the sudden switch from overshoot to undershoot takes place, which should be ignored.

4.1.4. Case (iv)

In Case (iv) tracking evaluation of the results of a real-time hybrid test is provided. The test was performed at the Lehigh University NEES RTMD facility and involved a SDOF steel moment resisting frame (MRF) as the nonlinear analytical substructure and a pair of elastomeric dampers (that was assumed to be installed on the web of the floor beams of the MRF) as the experimental substructure where the fundamental natural frequency of the test structure was found to be around 5.5 rad/sec. More information on the test setup, and testing method and results can be found in [3]. Fig. 9(a) displays the command and measured displacements for the first floor obtained from the real-time hybrid test, the corresponding SSP can be seen in Fig. 9 (b). The experimental substructure exhibits nonlinear behaviour and the hysteresis loops are provided in Fig. 10 (c). Tracking performance evaluation using HSEM (Fig. 9 (d)) reveals that there is a time delay between the command and measured signals.

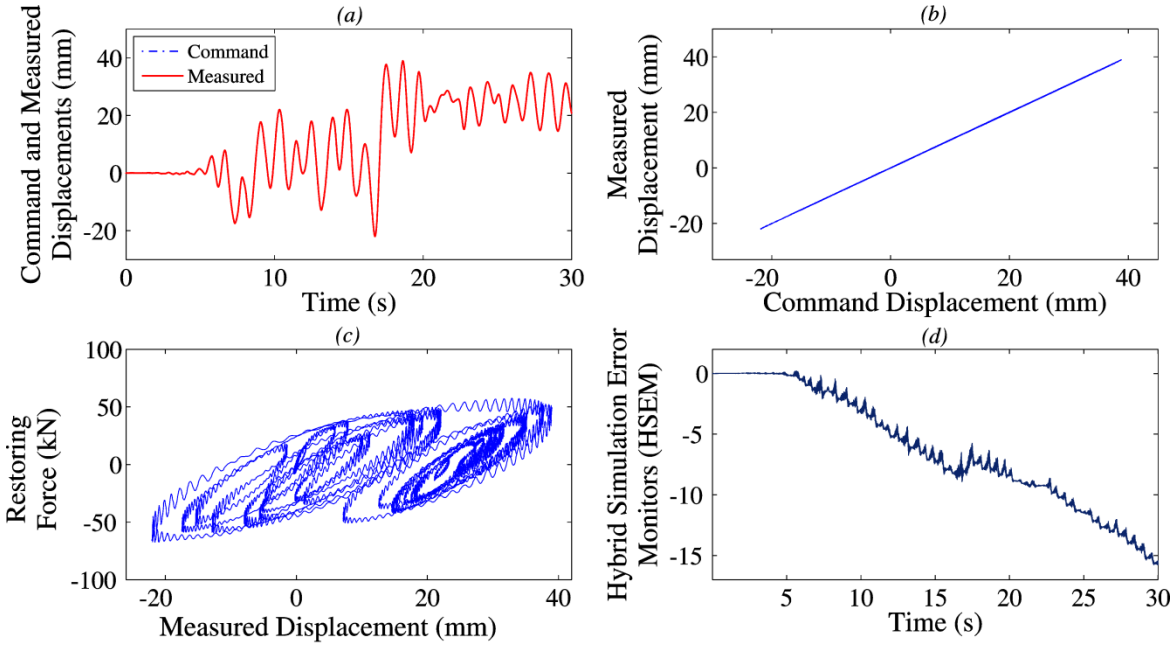

Fig. 9. HSEM Tracking evaluation for Case (iv) [3]

Phase and amplitude errors are also quantified in Fig. 10. To verify the PAEI results enlarged time windows are investigated in Fig. 11.

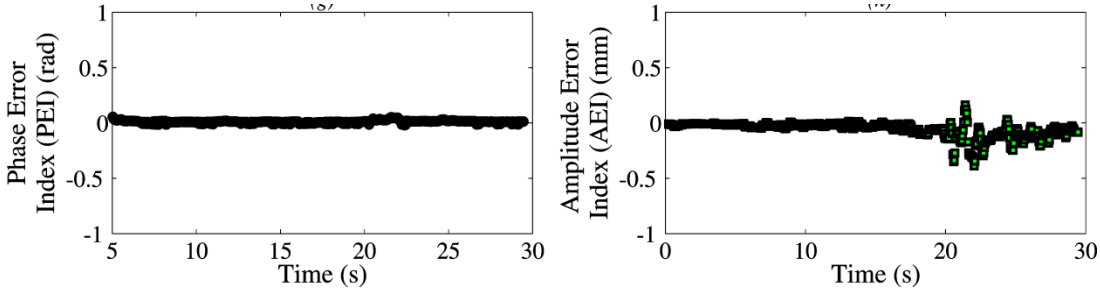

Fig. 10. PAEI Tracking evaluation for Case (iv) [3]

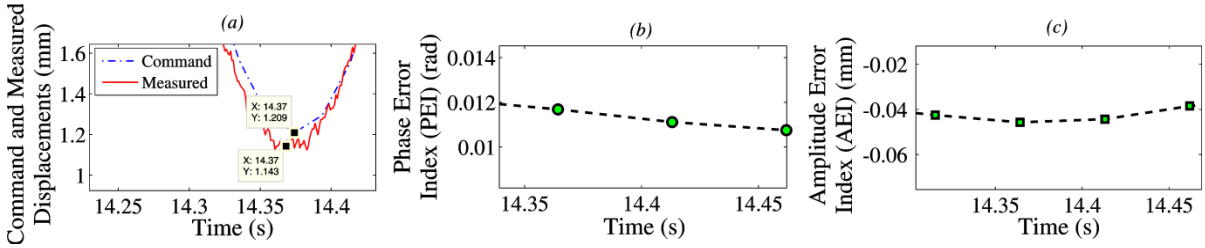

Fig. 11. Enlarged time windows to verify PAEI results for Case (iv) [3]

Fig. 11(a) shows the enlarged view of command and measured displacements from Fig. 9(a) around 14.35 sec where a lumped overshoot error of 0.07 mm can be observed. The enlarged view of AEI around 14.35 sec (Fig. 11(b)) has an acceptable agreement with the observed amplitude error. Using the fundamental natural frequency of the test structure considered in Case (iv) (i.e., 5.5 rad/sec) the delay observed in Fig. 11(a) translates into a time delay of 0.002 sec (or $2\Delta t$), which is in a good agreement with the results in Fig. 9(a).

4.2. FREQUENCY DOMAIN-BASED ERROR INDICATORS (FDB)

4.2.1. Case (v)

Two scenarios are considered for this case. In the first scenario, using the Simulink model of the inner loop, the effectiveness of the FDB error indicators in handling the signals with noise is studied. A comparison is made between the results obtained from the proposed FDB indicators and other available indicators (i.e., TI and PAEI) in order to evaluate the performance of the FDB error indicators. The predefined displacements are shown in Equations 8 and 9:

$$u_c = cos(\pi t) + K \times \{noise\} \quad (8)$$

$$u_m = 2\, cos(\pi[t + 25/1024]) + K \times \{noise\} \quad (9)$$

In Equations 8 and 9, a random number generator with a Gaussian distribution is used to consider the noise effects where the random number changes between zero and one and the multiplier K is assumed to be 0.10 mm. Time history and SSP of the u_c and u_m signals are shown in Fig. 12(a) and 12(b), respectively. TI and estimated amplitude ratio and phase error are also shown in Fig. 12. Note that $\phi = 0 - \pi \times [25/1024] = -0.077$ and $\Delta A = 0.5$. By comparing the results in Fig. 12(d) and 12(e) with the known errors, it can be seen that despite the relatively

high introduced noise level, FDB indicators can estimate the errors with an acceptable level of accuracy.

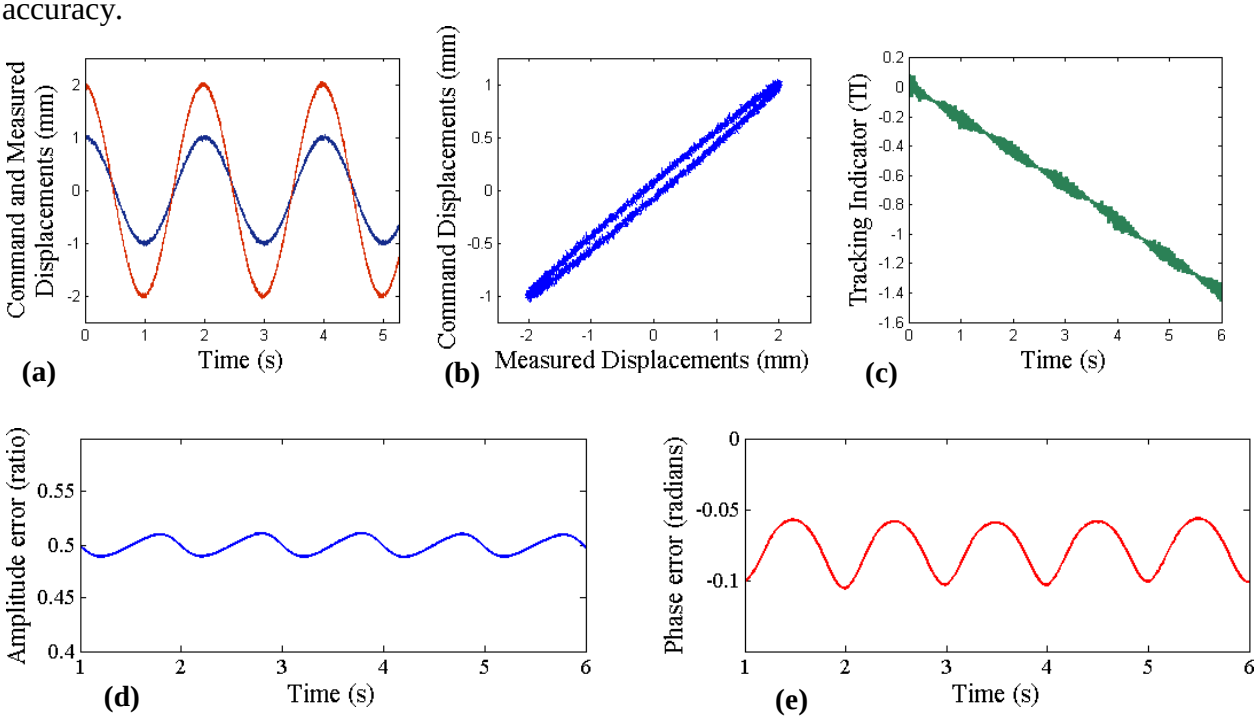

Fig. 12. Effectiveness of the FDB error indicators in dealing with noise: d) amplitude ratio and e) phase error of the signals [5]

4.2.2. Case (vi)

In Case (vi), it has been shown that the amplitude of the command displacements affects the accuracy of the some of the existing error indicators such as TI and HSEM. To investigate this, the amplitudes of the predefined command and measured displacements in Case (vi) are changed linearly with time. This variation is shown in Equation 10 and 11:

$$u_c = \{0.1t\} \times 2.5\ sin(3\pi t + \phi_c) \quad (10)$$

$$u_m = \{0.1t\} \times 2.0\ sin(3\pi t + \phi_m) \quad (11)$$

where, ϕ_c and ϕ_m are 0.092 and 0.369 radians, respectively. Thus, the amplitude ratio for this set of command and measured signals is equal to 1.25. Similarly, the phase error for this case is equal to -0.277 rad or -15.82 deg. Fig. 13 shows time histories of command and measured displacements (Fig. 13(a)), the corresponding synchronization subspace plot (Fig 13(b)), TI (Fig. 13(c)) and PAEI (Fig 13(d) and 13(e)) for this case. FDB indicators are also plotted in Fig. 13(f) and 13(g). Since all the command displacements considered in Fig. 13 have the same frequency and a constant time delay, the phase between the command and measured displacements estimated by TI, PAEI and FDB error indicators should be constant and the same. However, as discussed above, TI for each case is changing, implying that the slope of the tracking indicator is affected by the amplitude of the command displacement.

Table 3 compares the averaged FDB error indicators (from Fig. 13(f) and 13(g)) with the FEI error indicators. The known values of the amplitude and phase errors are also provided in the

table. FDB indicators are able to accurately quantify both the phase and amplitude errors and are in agreement with the values of the known errors and those measured by FEI.

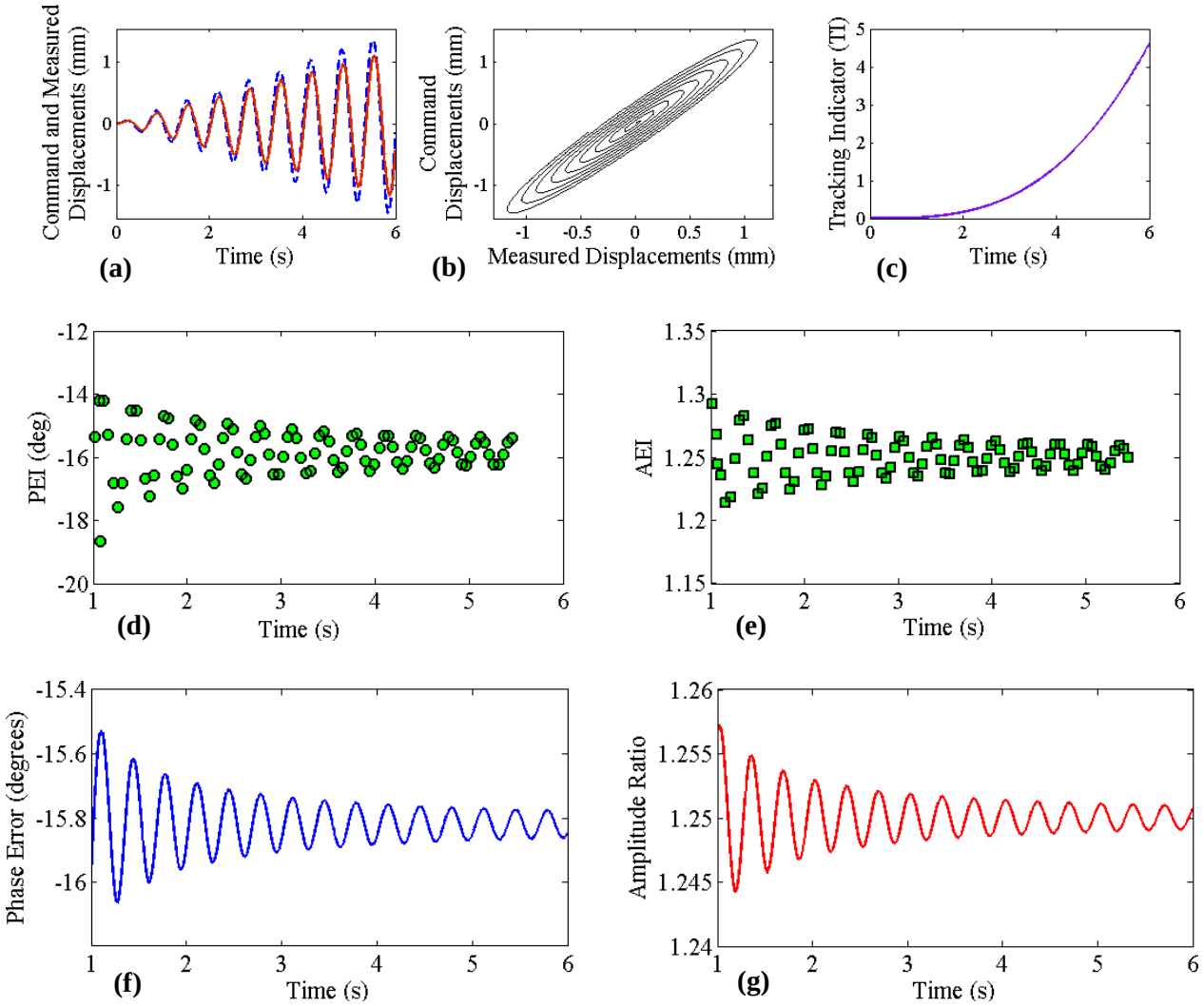

Fig. 13. Comparison between FDB and other error indicators for signals with time-varying amplitudes [5]

Table 3. Comparison between FDB and FEI error indicators with the exact solution for Case (vi) [5]

	Known values	Averaged FDB indicators	FEI indicators
Amplitude Ratio	1.25	1.245	1.250
Phase Error (deg)	-15.82	-15.749	-15.871

4.2.3. Case (vii)

In this case, in order to assess the accuracy of the FDB error indicators in quantifying the actuator tracking error, results from a real-time hybrid simulation are evaluated. The experiment was performed at the Lehigh University NEES RTMD facility and involved an SDOF steel moment resisting frame as the nonlinear analytical substructure and a pair of elastomeric

dampers as the experimental substructure. This particular real-time hybrid simulation result corresponds to another experiment with the same test setup explained in Case (iv). Recorded measured and command displacements are evaluated using TI, θ_{pc} [4] and HSEM. Fig. 14(a) shows the command and measured displacements obtained from the real-time hybrid simulation and the enlarged windows of these signals around 19.53 s and 23.35 s are shown in Fig. 14(c) and 14(d), respectively. In addition, the experimental substructure exhibits nonlinear behaviour and the hysteresis loops are provided in Fig. 14(b).

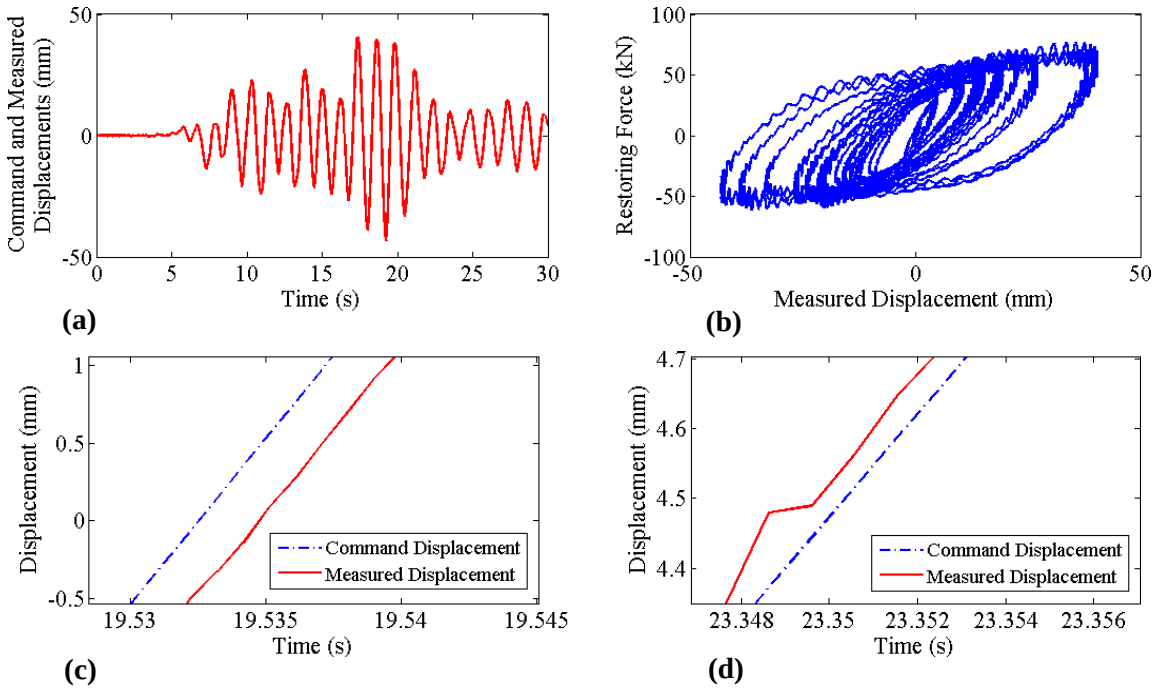

Fig. 14. Command and measured displacement time histories and hysteresis loop for Case (v) [5]

An important property of both HSEM and TI is their ability to qualitatively determine the phase error type. The negative and positive global slope of these plots corresponds to phase lead and phase lag, respectively. This test is particularly important because as shown in Fig. 15(a) and 15(b), the results of previous studies showed that the phase error switches from lead to lag to lead during the experiment. This is consistent with the observations in Fig 14(c) and 14(d). The slope of TI does not provide any information about the amplitude errors.

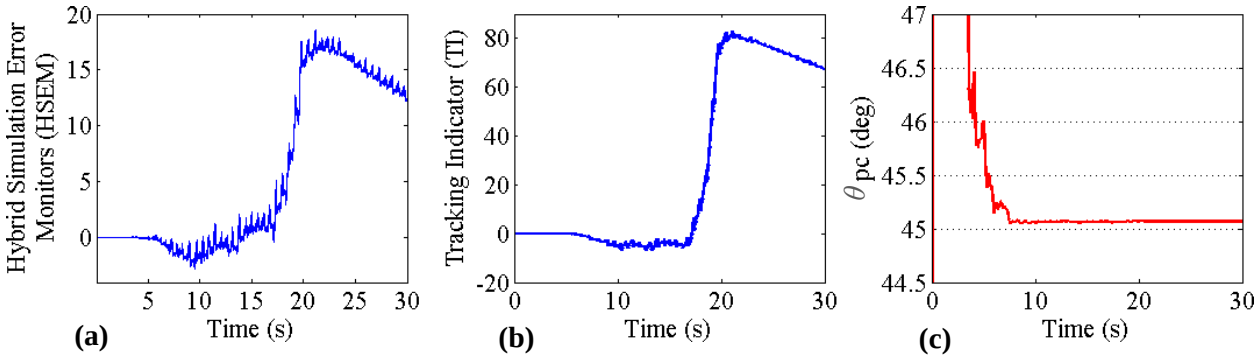

Fig. 15. Evaluation of the tracking errors using available methods: a) HSEM, b) TI and c) θ_{pc} [5]

Fig. 16(a) and 16(b) show the FDB error indicators for Case (vii). A closer look at Fig. 16 indicates that FDB error indicators successfully distinguish between lag and lead, and overshoot and undershoot errors. In other words, Fig. 16(a) shows that sign of the FDB phase error indicator is positive for the first portion of the signal and it becomes negative between the 16.5 and 21 seconds and then finally it changes to positive after the 21st second. This is in agreement with the observations from TI and HSEM. The amplitude error in Fig. 16(b) is also smaller than 1 which indicates an overshoot error.

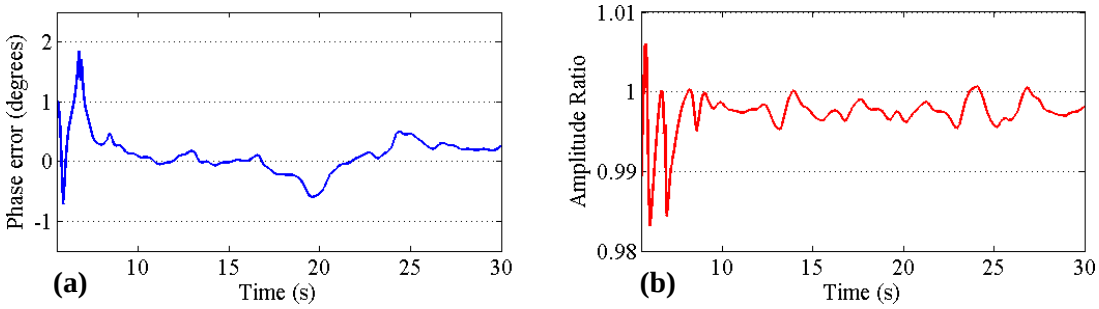

Fig. 16. FDB error indicators for Case (v) [5]

Moreover, using the fundamental natural frequency of the test structure considered in Case (vii) (i.e., 5.5 rad/s) the 0.002 s time delay observed in Fig. 14(c) translates into a -0.65 deg phase error, which is in good agreement with the results in Fig. 16(a) at around 19.53 s.

It is shown here that FDB error indicators can uncouple the phase and amplitude errors and can accurately quantify them. As such, their performance is superior in comparison to the previous indicators. In 2014, FDB error indicators were successfully implemented in real-time, and incorporated into the control loop of an adaptive controller (i.e., 2DOF controller). More information about the incorporation of these indicators into the controller and their experimental validation could be found in [5].

5. SUMMARY

One of the key factors in obtaining reliable hybrid simulation results is the accuracy of the servo-hydraulic actuator in tracking the command displacements. In recent years, several tracking error indicators were developed to assess the accuracy of actuator control in hybrid simulations. Some of these measures were published in the NEEShub [1]. This document introduced two additional sets of indicators (PAEI and FDB error indicators). PAEI are derived based on the characteristics of the SSP of the command and measured displacements and FDB error indicators are formulated in frequency domain. Both of these local response measures can uncouple and separately quantify the amplitude and phase errors. Moreover, both of these error indicators employ a moving window approach with proper windowing functions. This enables the FDB error indicators to be implemented and executed in real-time. As such, FDB indicators not only become online assessment tools that can assess the tracking performance of the hydraulic actuator as the real-time hybrid simulation progresses, but they can also be incorporated into the servo-hydraulic control law. Through several numerical simulations, the effects of the window size, windowing functions, noise, frequency, and amplitude characteristics of the signals processed were investigated through numerical simulations. The performance of PAEI and FDB error indictors are also investigated by processing command and measured

displacements from a real-time hybrid simulation performed at Lehigh NEES RTMD site. It is shown that PAEI are able to quantify the errors, even when the test structure considered exhibit nonlinear behaviour and in the presence of noise. It is also shown that unlike energy-based measures and TI, PAEI and FDB error indicators results are unaffected by the amplitude of the command displacements. As such, the two discussed error measures can serve as standard indicators to compare the accuracy of the real-time test results which have considerably different command displacement histories.

REFERENCES

1. Christenson, R., Dyke, S., Zhang, J., Mosqueda, G., Chen, C., Nakata, N., Laplace, P., Song, W., Chae, Y., Marshall, G.A., Ou, G., Riascos Gonzales, C.A., and Song., C. (2014). "Hybrid simulation: a discussion of current assessment measures," https://nees.org/resources/12876.
2. Horiuchi, T., Inoue, M., Konno, T., and Namita, Y. (1999). "Real-time hybrid experimental system with actuator delay compensation and its application to a piping system with energy absorber." *Earthquake Engineering and Structural Dynamics*, 28(10), 1121–1141.
3. Mirza Hessabi, R., and Mercan, O. (2012). "Phase and amplitude error indices for error quantification in pseudodynamic testing." *Earthquake Engineering and Structural Dynamics*, 41(10), 1347–1364.
4. Mercan, O., and Ricles, J.M. (2007). "Stability and accuracy analysis of outer loop dynamics in real-time pseudodynamic testing of SDOF systems." *Earthquake Engineering and Structural Dynamics*, 36(11), 1523–1543.
5. Mirza Hessabi, R., Ashasi-Sorkhabi, A., and Mercan, O. (2014). "A new tracking error-based adaptive controller for servo-hydraulic actuator control." *Journal of Vibration and Control*, 1–17. DOI: 10.1177/1077546314548205.
6. Guo, T., Chen, C., Xu, W., and Sanchez F. (2014). "A frequency response analysis approach for quantitative assessment of actuator tracking for real-time hybrid simulation." *Smart Materials and Structures*, 23(4).
7. Gao, X. (2012) "Development of a Robust Framework for Real-Time Hybrid Simulation: From Dynamical System, Motion Control to Experimental Error Verification", Doctoral Dissertation, Purdue University, West Lafayette, IN.
8. Phillips, B.M., and Spencer, B.F. (2011) "Model-Based Feedforward-Feedback Tracking Control for Real-Time Hybrid Simulation", Newmark Structural Engineering Laboratory Report Series, University of Illinois at Urbana-Champaign, Urbana, IL, No. 28.
9. Mosqueda, G., Stojadinovic, B., and Mahin, S.A. (2007a). "Real-time error monitoring for hybrid simulation. Part I: Methodology and Experimental Verification." Journal of Structural Engineering, 133(8), 1100-1108.
10. Mosqueda, G., Stojadinovic, B., and Mahin, S. A. (2007b). "Real-time error monitoring for hybrid simulation. Part II: Structural response modification due to errors." Journal of Structural Engineering, 133(8), 1109-1117.
11. Ahmadizadeh, M., and Mosqueda, G. (2009). "Online energy-based error indicator for the assessment of numerical and experimental errors in a hybrid simulation." Engineering Structures, 31(9), 1987-1996.